Analysis of the Jahn-Teller Effect in Matrix Isolated Cyclooctatetraene Mononegative Ion Using Magnetic Circular Dichroism Spectroscopy

Cindy Samet,*,† Janna L. Rose,‡,⊥ Susan B. Piepho,*,§ Joseph Laurito,‡ Lester Andrews,‡ and Paul N. Schatz*,‡

Contribution from the Chemistry Department, Dickinson College, Carlisle, Pennsylvania 17013, the Chemistry Department, University of Virginia, Charlottesville, Virginia 22901, and the Chemistry Department, Sweet Briar College, Sweet Briar, Virginia 24595

Received May 19, 1994[⊗]

Abstract: The magnetic circular dichroism (MCD) and absorption spectrum of cyclooctatetraene mononegative ion (COT^-), prepared by co-condensing Cs atoms with COT neutral, have been measured in argon matrices over the temperature range 1.69-21.9 K. Attention has been focused on the first allowed electronic transition, which shows clearly resolved vibronic structure. The MCD spectrum shows a strongly temperature-dependent signal which oscillates in sign. These observations show unambiguously that COT^- in its ground state is within the dynamic range of D_{8h} (or C_{8v}) symmetry and that the electronic transition involves Jahn-Teller coupling. The data can be explained if the ground and excited electronic states are assumed to have respective point group symmetries D_{8h} and D_{4h} (or D_{2d}) with significant Jahn-Teller effects in both states. To explain the magnitude and temperature dependence of the MCD, it is also necessary to include spin-orbit and crystal field perturbations in the ground state. The ground state can be pictured as strongly trapped in two Kekule-like structures separated by a Jahn-Teller barrier of $\approx$1440 cm^{-1} with tunneling possible between the two structures. The ground state parameters are $\nu_{JT}(b_{1g}) \approx 1140$ cm^{-1}, $E_{JT} \approx 1440$ cm^{-1}, and crystal field $\Delta(b_{1g}) \approx 13$ cm^{-1}, with Ham-effect quenching of the orbital angular momentum by the factor $e^{-\lambda^2_{JT}} = 0.08$. The excited state Jahn-Teller parameters are $\nu_{JT} \approx 270$ cm^{-1}, $E_{JT} \approx 130$ cm^{-1}. It is shown that the Cs^+ counterion, which must be present, does not affect the analysis in any essential way.

I. Introduction

Since its discovery by Willstater and Waser[1] eight decades ago, cyclooctatetraene and its derivatives and ions have been important from a theoretical and synthetic standpoint. Neutral cyclooctatetraene (COT) exists in a strain-free, non-planar D_{2d} "tub" conformation, and ring inversion and bond-shift processes can occur via planar transition states with alternating bond lengths (D_{4h} symmetry) and equal bond lengths, respectively.[2] Therefore, considerable attention has been focused on the existence and synthesis of species containing planar, conjugated eight-membered-ring systems. In general, there are two ways to prepare planar COT species. The first is to synthesize cyclooctatetraenes that are constrained to planar conformations by small ring fusions.[3] (Pirrung et al.[4] have recently synthesized the first example of a class of cyclobutenocyclooctatetraenes that possesses both stability at room temperature and a carbon skeleton closer to planarity than any bicyclic cyclooctatetraene yet prepared.) The second is to reduce neutral COT to either its radical anion (COT^-) or Hückel dianion (COT^{2-}). It has been stated that, "it is well-known that complete ring flattening occurs when COT is reduced to either its radical anion (monoanion) or Hückel dianion, and when it acts as an $\eta 8$ ligand in metal complexes."[5] Studies such as those done by Pirrung and others complement studies of COT ions because they provide insight into the structural changes occurring prior to electron transfer to form the COT radical anion. Presently it is believed that electron transfer awaits ring flattening which affords the planar radical anion.

X-ray[6] and electron diffraction studies[7-9] of COT show unambiguously that the eight-membered ring exists in a buckled D_{2d} tub form possessing alternating single and double bonds. Although neutral COT is a $4n$-electron system, and a significant loss in resonance energy is predicted for a nonplanar structure of alternating single and double bonds, the D_{2d} molecule is indeed quite stable.[5] Early studies[10,11] indicated that the dianion COT^{2-} has D_{8h} symmetry with such aromatic features as a ring current, and later X-ray studies confirmed that D_{8h} structure in potassium diglyme COT^{2-} crystals.[12,13] Katz[10] has also shown that COT has a higher electron affinity than do most olefins. These findings support the Hückel $(4n + 2)$-rule for aromatic stability. For planar COT^-, molecular orbital theory in the Hückel approximation predicts an orbitally degenerate electronic ground state subject to Jahn-Teller distortions. Since the

† Dickinson College.
‡ University of Virginia.
⊥ Present address: Rayovac Corporation, Madison, WI.
§ Sweet Briar College.
⊗ Abstract published in *Advance ACS Abstracts*, November 1, 1994.

(1) Willstatter, R.; Waser, E. *Ber.* **1911**, *44*, 3423.
(2) Dewar, M. J. S.; Merz, K. M., Jr. *J. Chem. Phys.* **1985**, *89*, 4739.
(3) Britton, W. E.; Ferraris, J. P.; Soulen, R. L. *J. Am. Chem. Soc.* **1982**, *104*, 5322.
(4) Pirrung, M. C.; Krishnamurthy, N.; Nunn, D. S.; McPhail, A. T. *J. Am. Chem. Soc.* **1991**, *113*, 4910.
(5) Fray, G. I.; Saxton, R. G. *The Chemistry of Cyclo-octatetraene and its Derivatives*; Cambridge University Press: New York, 1978.
(6) Bordner, J.; Parker, R. G.; Stanford, R. H. *Acta Crystallogr.* **1972**, *B28*, 1069.
(7) Karle, I. L. *J. Chem. Phys.* **1952**, *20*, 65.
(8) Bastiansen, O.; Hedberg, L.; Hedberg, K. *J. Chem. Phys.* **1957**, *27*, 1311.
(9) Traetteberg, M. *Acta Chem. Scand.* **1966**, *20*, 1724.
(10) Katz, T. J. *J. Am. Chem. Soc.* **1960**, *82*, 3784.
(11) Strauss, H. L.; Katz, T. J.; Fraenkel, G. K. *J. Am. Chem. Soc.* **1963**, *85*, 2360.
(12) Noordik, J. H.; van den Hark, Th. E. M.; Mooij, J. J.; Klaassen, A. A. K. *Acta Crystallogr.* **1974**, *30*, 833.
(13) Goldberg, S. Z.; Raymond, K. N.; Harman, C. A.; Templeton, D. H. *J. Am. Chem. Soc.* **1974**, *96*, 1348.

0002-7863/94/1516-11109$04.50/0

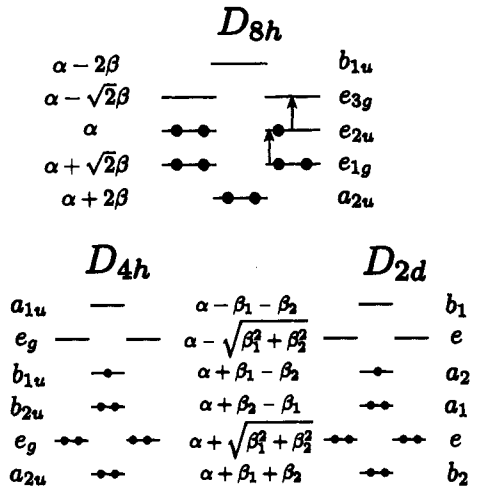

Figure 1. Hückel energy levels for COT assuming different possible symmetries.[14] The electron occupancy shown corresponds to COT^-. The vertical arrows show the two most important excitations responsible for the $^2E_{2u} \rightarrow {}^2E_{1g}$ transition discussed in this paper. (The irrep labels b_1 and b_2 are interchanged with respect to those of Kimmel and Strauss[14] because we define C'_2 to *bisect* a C–C bond (Table 1 and Figure 4).)

added electron in COT^- enters a nonbonding orbital of the D_{8h} structure and an antibonding orbital of the D_{2d} structure, it should stabilize the former (Figure 1).

Kimmel and Strauss[14] concluded from the electronic spectrum and calculations assuming several possible geometries that the anion "differs little, if at all, from D_{8h} symmetry." Later, Shida and Iwata,[15] Banerjee and Simons,[16] and Dvorak and Michl[17] studied the anion radical in glasses at 77 K. These spectroscopic studies suggest that COT^- is planar and rigid, at least as it exists in the glass. In particular, the near "mirror-image" symmetry between the emission and absorption spectra recorded by Dvorak and Michl lead them to conclude that the rigidity is preserved in the lowest excited state whose equilibrium geometry is therefore similar to the ground state.

ESR studies[18,19] also indicate D_{8h} symmetry for the monoanion. The ESR spectrum reported by Katz and Strauss[18] has nine equidistant hyperfine lines 3.21 G apart, which is the structure expected for a planar radical with eight equivalent ring protons and a spin density of 1/8 on each carbon atom. The hyperfine splitting corresponds to the usual Q value of -25 found for the negative ions of planar aromatic hydrocarbons. Also, Katz and Strauss argue that the high rate of electron exchange between the radical and the dianion implies that the two species have similar structures. Temperature-dependent ESR studies[19] on COT^- focus on the effects of ion pairing.

McLachlan and Snyder[20] also addressed the issue of planarity in COT^-. They concluded that the sharper ESR spectrum of COT^- resulting from smaller fluctuations in spin density as compared to benzene or coronene negative ions is consistent with a planar structure and an orbitally degenerate ground state subject to a Jahn–Teller effect. They estimate a Jahn–Teller energy of $\approx$825 cm^{-1} with the Jahn–Teller stretching vibration predominant. Thus two Kekule–like configurations are predicted about 825 cm^{-1} below the D_{8h} configuration with alternating bond lengths of 1.410 and 1.36 Å.

More recent *ab initio* calculations support the view of McLachlan and Snyder. Trindle and Wolfskill[21] compute a minimum energy D_{4h} structure for COT^- with alternating C–C bond lengths of 1.36 and 1.41 Å, in contrast to previous semiempirical calculations which predict a slight D_{2d} distortion. In addition, *ab initio* calculations by Hammons et al.[22] also suggest a D_{4h} structure for the monoanion. Their optimization of a nonplanar, bond-length-alternated D_{2d} structure converged back to a D_{4h} structure with C–C bond lengths almost identical to those reported by Trindle and Wolfskill.

Although the operation of the Jahn–Teller effect in organic molecules and especially in negative aromatic ions has been the subject of extensive theoretical and experimental work, relatively few studies exist where theory may be compared directly with experiment. For example, ESR experiments yield information about ground state properties, but these can be assessed only indirectly through small spin–orbit couplings. The present study employs magnetic circular dichroism (MCD) spectroscopy, which unlike ESR, shows strong temperature effects if the ground state is orbitally degenerate. This study was undertaken to elucidate the structure of the COT radical anion and to investigate the nature and strength of the Jahn–Teller effect. The matrix isolation technique proves ideal since the guest ions can be generated *in situ* in an almost inert host, and thus important spectral features are not obscured by solvent effects.

II. Experimental Section

Our experimental procedures and equipment have been described in detail previously.[23] The matrix sample is prepared in a continuous flow (CF) cryostat and is subsequently injected into a split-coil magnet system. Sample temperatures can be accurately monitored since the matrix is immersed either in liquid He ($\leq$4.2 K) or He exchange gas ($\geq$4.2 K). MCD and double-beam absorption data are recorded simultaneously, ensuring that precisely the same sample is examined in both measurements.

The cyclooctatetraene was obtained from the Alfa Chemical Company and used without further purification. To prepare the Ar/COT mixture, a coldfinger containing COT liquid was attached to a vacuum line, frozen, evacuated, and then thawed. The COT vapors were then allowed to expand into a stainless steel can. The Ar gas (Matheson) was added to the can to obtain Ar/COT in a ratio of about 30/1. Spectra of COT^- were obtained by codeposition of Li, Na, K, or Cs atoms with the COT/Ar mixture. The absorption spectra were qualitatively similar for each of the alkali metals with a slight red shift as the size of the metal cation increases. However, the vibronic fine structure was far better resolved in Cs/COT^- than in any of the others, and only in the Cs/COT^- do we observe a temperature-dependent MCD (see later). The cesium was produced by loading a Knudsen cell with lithium metal (Fisher Scientific) and cesium chloride (Fisher) and heating the mixture in a glass tube until an exchange of Li and Cs atoms began. Following this procedure, which is done prior to the matrix deposition, the Knudsen cell is transferred to the CF cryostat oven so that the Cs atoms may be codeposited with the Ar/COT mixture. The Knudsen cell was heated to about 340 °C during the deposition. The Cs and gas mixture was deposited for a total of 40 min. The matrix was pale yellow.

III. Results

A survey of the $Cs/COT^-/Ar$ MCD and absorption spectra is shown in Figure 2. These data were recorded at relatively low resolution with the deposition window mounted *in vacuum* in the bore of a single-coil solenoid. The sample temperature, which cannot be accurately measured in such a configuration,[23] was estimated as about 6–8 K. The absorption is characterized

(14) Kimmel, P. I.; Strauss, H. L. *J. Phys. Chem.* **1968**, *72*, 2813.
(15) Shida, T.; Iwata, S. *J. Am. Chem. Soc.* **1972**, *95*, 3473.
(16) Banerjee, A.; Simons, J. *J. Chem. Phys.* **1978**, *69*, 5538.
(17) Dvorak, G.; Michl, J. *J. Am. Chem. Soc.* **1976**, *98*, 1080.
(18) Katz, T. J.; Strauss, H. L. *J. Chem. Phys.* **1960**, *32*, 1873.
(19) Smentowski, F. J.; Stevenson, G. R. *J. Phys. Chem.* **1969**, *73*, 340.
(20) McLachlan, A. D.; Snyder, L. C. *J. Chem. Phys.* **1962**, *36*, 1159.
(21) Trindle, C.; Wolfskill, T. *J. Org. Chem.* **1991**, *56*, 5426.
(22) Hammons, J. H.; Hrovat, D. A.; Borden, W. T. *J. Am. Chem. Soc.* **1991**, *113*, 4500.
(23) Rose, J.; Smith, D.; Williamson, B. E.; Schatz, P. N.; O'Brien, M. C. M. *J. Phys. Chem.* **1986**, *90*, 2608.

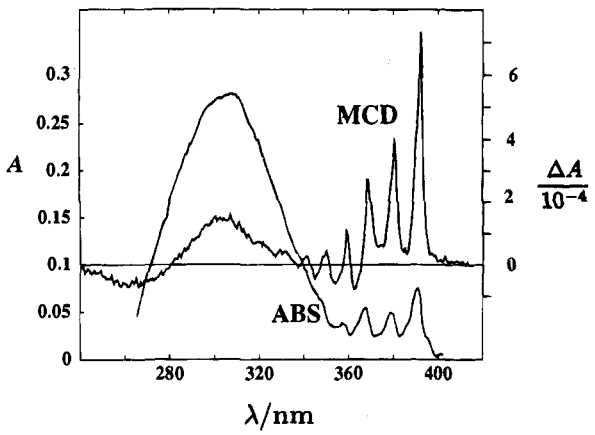

Figure 2. Low-resolution survey spectra of Cs/COT⁻/Ar with temperature in the approximate range 6−8 K. The lower spectrum is the absorption in optical density units (left scale), and the upper spectrum is the MCD in optical density units per tesla (right scale).

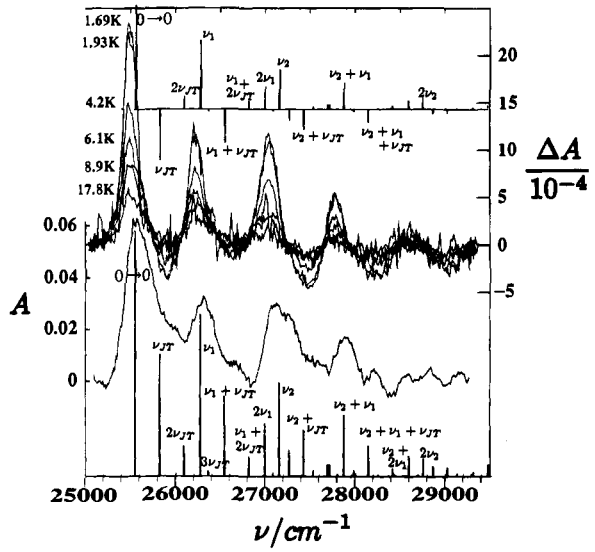

Figure 3. High-resolution absorption and MCD spectra of Cs/COT⁻/Ar as recorded in the split-coil system where temperature could be accurately monitored. Absorption and MCD units are as in Figure 1. The temperature dependence of the MCD is shown in the upper panel where, for clarity, the spectra recorded at 2.44 and 21.9 K are not shown. The amplitudes of the MCD spectra vary inversely with temperature. The lower panel shows the absorption spectrum averaged over the experimental temperature range. The stick spectra summarize the vibronic assignments made in this work (Table 2). The heights of the sticks are proportional to absorbances (lower set) and MCD (upper set), calculated as described in Section IV.4.

by two transitions, one of which shows resolved vibronic structure between 350 and 400 nm, while the other is broad and featureless with a maximum at ~300 nm. The absorption spectrum agrees well with the literature[15−17] though we are limited by the relatively low yields of COT⁻ achievable in the matrix experiment. The corresponding MCD is broad and relatively weak for the higher energy band, and may be complicated by the presence of COT^{2-} which also absorbs in this region. However, the lower energy band shows well-resolved vibronic structure which is undoubtedly attributable to the COT⁻ species. This paper focuses exclusively on this latter region.

The region of interest is shown at higher resolution in Figure 3 following injection into the split-coil system where accurate temperature monitoring is possible. The absorption is very weak (peak optical density ~0.06), with no discernable temperature dependence. The absorption spectrum shown in Figure 3 is the average of the data collected over the temperature range studied. This improves the signal-to-noise significantly. The MCD, on the other hand, shows a strong inverse temperature dependence with far better resolved vibronic structure. *The observation of a pronounced temperature dependence in the MCD is the crucial underpinning of our entire analysis.* We shall show that this dependence is the consequence of a near vibronic degeneracy in the ground manifold and consequently the existence of a residual orbital angular momentum. (No temeprature dependence at all was observed in the corresponding MCD spectrum of $Na^+/COT^-/Ar$, a point on which we comment later.) The existence of ground state orbital angular momentum means in turn that the electronic ground state of COT⁻ is within the dynamic range of D_{8h} (or C_{8v}) symmetry. This is evident by inspection of Figure 1 since one observes that the ground states of D_{4h} (or C_{4v}) or D_{2d} COT⁻ have zero orbital angular momentum, and hence the corresponding MCD would be temperature independent. (Spin degeneracy is still present, but spin can be ignored in MCD spectroscopy in the absence of spin-orbit coupling (Reference 24, section 11.3). If the ground state has zero orbital angular momentum, ground state spin-orbit coupling will be exceedingly small. This is to be contrasted with the D_{8h} case discussed in Section V.5 where spin-orbit coupling plays a crucial role.)

IV. Interpretation of Spectra

1. The Rigid Shift and Born−Oppenheimer Assumptions. Let us start by examining the consequences of assuming that our COT⁻ species has exact D_{8h} symmetry with negligible Jahn−Teller coupling in both the ground and excited states. For the fully-allowed electronic transition (Figure 1), $^2E_{2u} \rightarrow {}^2E_{1g}$, making the rigid-shift and Born−Oppenheimer approximations, the relevant MCD and absorption expressions would be,[24]

$$\Delta A/\mathcal{E} = \gamma\mu_B B[\bar{\mathcal{A}}_1(-(\partial f(\mathcal{E})/\partial\mathcal{E}) + (\bar{\mathcal{B}}_0 + \bar{\mathcal{C}}_0/kT)f(\mathcal{E})]$$

$$A/\mathcal{E} = \gamma\bar{\mathcal{D}}_0 f(\mathcal{E}) \qquad (1)$$

with

$$\bar{\mathcal{A}}_1 = \frac{i}{3|A|}\sum_{\substack{\alpha\alpha'\\ \lambda\lambda'}}(\langle J\lambda|\mathbf{L}+2\mathbf{S}|J\lambda'\rangle\delta_{\alpha\alpha'} - \langle A\alpha'|\mathbf{L}+2\mathbf{S}|A\alpha\rangle\delta_{\lambda\lambda'})\cdot(\langle A\alpha|\mathbf{m}|J\lambda\rangle\times\langle J\lambda'|\mathbf{m}|A\alpha'\rangle)$$

$$\bar{\mathcal{B}}_0 = \frac{2\mathrm{Im}}{3|A|}\sum_{\alpha\lambda}\left[\sum_{\substack{K\kappa\\(K\neq A)}}\frac{\langle K\kappa|\mathbf{L}+2\mathbf{S}|A\alpha\rangle}{W_K - W_A}\cdot(\langle A\alpha|\mathbf{m}|J\lambda\rangle\times\langle J\lambda|\mathbf{m}|K\kappa\rangle) + \sum_{\substack{K\kappa\\(K\neq J)}}\frac{\langle J\lambda|\mathbf{L}+2\mathbf{S}|K\kappa\rangle}{W_K - W_J}\cdot(\langle A\alpha|\mathbf{m}|J\lambda\rangle\times\langle K\kappa|\mathbf{m}|A\alpha\rangle)\right] \qquad (2)$$

$$\bar{\mathcal{C}}_0 = \frac{-i}{3|A|}\sum_{\alpha\alpha'\lambda}\langle A\alpha'|\mathbf{L}+2\mathbf{S}|A\alpha\rangle\cdot(\langle A\alpha|\mathbf{m}|J\lambda\rangle\times\langle J\lambda|\mathbf{m}|A\alpha'\rangle)$$

$$\bar{\mathcal{D}}_0 = \frac{1}{3|A|}\sum_{\alpha\lambda}|\langle A\alpha|\mathbf{m}|J\lambda\rangle|^2$$

In these equations, $|A\alpha\rangle$ and $|J\lambda\rangle$ are respectively identified with

(24) Piepho, S. B.; Schatz, P. N. *Group Theory in Spectroscopy with Applications to Magnetic Circular Dichroism Spectroscopy*; Wiley: New York, 1983.

Table 1. Transformation Properties of D_8 Standard Basis Functions under the Group D_8 Generators and in Group D_4

D_8 function	operation $\hat{C}_8^z$	operation $\hat{C}_2^{\prime x a}$	$D_4^{b,c}$
A_1a_1	A_1a_1	A_1a_1	A_1a_1
A_2a_2	A_2a_2	$-A_2a_2$	A_2a_2
B_1b_1	$-B_1b_1$	B_1b_1	A_1a_1
B_2b_2	$-B_2b_2$	$-B_2b_2$	A_2a_2
E_11	$e^{-i\pi/4}E_11$	$-E_1 - 1$	$E1$
$E_1 - 1$	$e^{i\pi/4}E_1 - 1$	$-E_11$	$E - 1$
E_22	$e^{-i\pi/2}E_22$	$E_2 - 2$	$2^{-1/2}(B_1b_1 + B_2b_2)$
$E_2 - 2$	$e^{i\pi/2}E_2 - 2$	E_22	$2^{-1/2}(B_1b_1 - B_2b_2)$
E_33	$e^{-i3\pi/4}E_33$	$-E_3 - 3$	$E - 1$
$E_3 - 3$	$e^{i3\pi/4}E_3 - 3$	$-E_33$	$E1$
$\|JM\rangle^d$	$\|JM\rangle e^{-i\pi M/4\ d}$	$\|J - M\rangle e^{-i\pi J\ d}$	

[a] $\hat{C}_2^{\prime x}$ is perpendicular to $\hat{C}_8^z$ and *bisects* a C–C bond—see Figure 4. [b] $\hat{C}_2^{\prime}$ $(D_4) \equiv \hat{C}_2^{\prime x}(D_8)$—see Figure 4. [c] For example, $|E_22(D_8)\rangle = 2^{-1/2}(|B_1b_1(D_4)\rangle + |B_2b_2(D_4)\rangle)$. [d] J, M half-integer.

$|^2E_{2u} \pm 2\rangle$ and $|^2E_{1g} \pm 1\rangle$, γ is a collection of constants, μ_B is the Bohr magneton (0.467 cm^{-1}/T), B is the magnetic field in tesla, $f(\mathcal{E})$ is an *ad hoc*, normalized bandshape function, and $\bar{\mathcal{A}}_1$, $\bar{\mathcal{B}}_0$, $\bar{\mathcal{C}}_0$, and $\bar{\mathcal{D}}_0$ are the standard MCD and absorption parameters, the bars indicating an average over all orientations. Im designates imaginary part. If resolved vibronic structure is observed, then eq 1 (multiplied by an appropriate Franck–Condon factor) is applicable to each member of each totally symmetric progression.

To estimate relevant parameters, we use Hückel MOs. Our definition of standard basis functions is given in Table 1 using the coordinate system shown in Figure 4. Using Slater functions and a well-known formula[25] for calculating angular momentum matrix elements, we obtain the following results for the transition $^2E_{2u} \rightarrow {}^2E_{1g}$ (in units of $\hbar$):

$$\bar{\mathcal{C}}_0/\bar{\mathcal{D}}_0 = \langle (e_{2u}^3)^2E_{2u}2|L_z|(e_{2u}^3)^2E_{2u}2\rangle \equiv \bar{L}_Z = \langle e_{2u}2|l_z|e_{2u}2\rangle = 1.33$$

$$|e_{2u}2\rangle = (1/\sqrt{8})(\phi_1 - \phi_3 + \phi_5 - \phi_7) - (i/\sqrt{8})(\phi_2 - \phi_4 + \phi_6 - \phi_8) \quad (3)$$

where ϕ_i is a $2p_\pi$ orbital on carbon atom i numbered as in Figure 4. Note that eq 3 depends only on the symmetry of the excited state—not the degree of configuration interaction.

We may in turn estimate an experimental value for $\bar{\mathcal{C}}_0/\bar{\mathcal{D}}_0$ from a moment analysis of the band using the relation

$$0.467\left(\frac{\bar{\mathcal{B}}_0 + \bar{\mathcal{C}}_0/kT}{\bar{\mathcal{D}}_0}\right) = \frac{\int(\Delta A/\mathcal{E})\,d\mathcal{E}}{\int(A/\mathcal{E})\,d\mathcal{E}} \equiv \frac{M_0}{A_0} \quad (4)$$

where M_0 and A_0 are respectively the zeroth MCD (per tesla) and absorption moments and the integrations are over the entire band. A plot of the right-hand side of eq 4 *vs* $1/T$ is shown by the filled circles in Figure 5. From the slope of a least-squares linear fit of the data, we obtain the values $\bar{\mathcal{C}}_0/\bar{\mathcal{D}}_0 \approx 0.02$, $\bar{\mathcal{B}}_0/\bar{\mathcal{D}}_0 \approx 0.004$. The very low experimental value of $\bar{\mathcal{C}}_0/\bar{\mathcal{D}}_0$ ($\approx$0.02) *vs* a theoretical value of 1.33 (eq 3) suggests very strong quenching of the ground state orbital angular momentum, a phenomenon associated with a Jahn–Teller effect. (In principle, we could also determine $\bar{\mathcal{A}}_1/\bar{\mathcal{D}}_0$ by analyzing the first MCD moment, but in fact this is not feasible because this moment is *far more* sensitive to baseline uncertainties and to the fact that

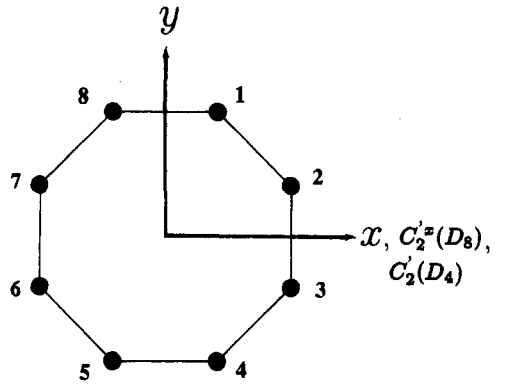

Figure 4. Coordinate system and numbering of carbon atoms. $\hat{C}_8^z$ and $C_2^{\prime x}$ are D_8 group generators; $\hat{C}_4^z$ and $C_2^{\prime}$ are D_4 group generators.

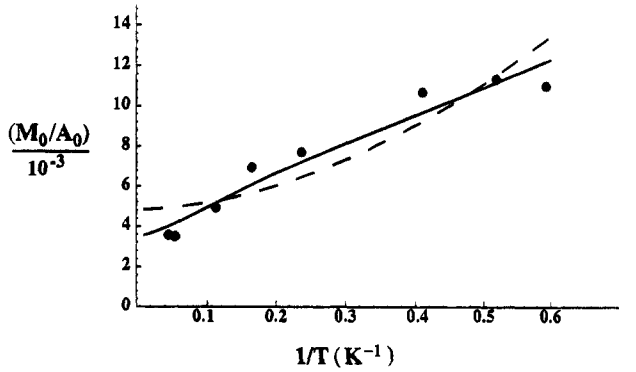

Figure 5. Ratio of zeroth MCD and absorption moments *vs* $1/T$. The filled circles are the experimental points, and the solid and dashed curves are respective best fits with and without a crystal field.

the blue end of the band overlaps with the broad tail of the much more intense $^2E_{2u} \rightarrow {}^2E_{3g}$ band.)

Conclusive evidence for Jahn–Teller activity is furnished by an examination of the absorption and particularly the MCD pattern (Figure 3). There are two obvious totally symmetric progressions in absorption, as has been noted by previous workers.[17] First there is a ~720 cm^{-1} (ν_1) mode built on the no-phonon band, and this pair is repeated twice with decreasing intensity in a ~1600 cm^{-1} (ν_2) mode. This pattern is mirrored in the MCD, as would be expected for totally symmetric progressions. However, there is a low energy shoulder in absorption (ν_{JT}), also noted in earlier work,[17] which is manifested in the MCD by an oppositely-signed (negative) $\bar{\mathcal{C}}$ term. *This is the unambiguous signature of a non-totally symmetric vibration*, and it is the sign calculated for either of the Jahn–Teller-active vibrations, b_{1g} or b_{2g} (see later).

We show in the next section that the vibronic pattern just described requires that the *excited electronic state* have a point group symmetry lower than D_{8h} and that the 270 cm^{-1} shoulder in fact arises from an *excited state* Jahn–Teller effect.

2. Normal Modes in COT$^-$. We observe in the absorption and MCD spectra two totally symmetric modes with frequencies of about 720 and 1600 cm^{-1} and a Jahn–Teller mode of frequency ~270 cm^{-1}. If we assume that COT^- has D_{8h} point group symmetry, straightforward group-theoretic procedures show that this molecule has (among others) the following normal modes: two totally symmetric (a_{1g}), two b_{1g}, two b_{2g}, and four e_{2g} modes. It is very illuminating to identify these modes with the fundamental frequencies expected for COT^-. Experimental data are available for only a few of the 42 normal modes, so we compare primarily with a Gaussian 90 *ab initio* geometry-optimized calculation (HF/6-31G//HF/6-31G).[26] Frequencies are

(25) McHugh, A. J.; Gouterman, M.; Weiss, C. *Theor. Chim. Acta* **1972**, *24*, 346.

(26) Maclagan, R. G. A. R. Department of Chemistry, University of Canterbury; unpublished work.

Table 2. Important Fundamental Frequencies of COT^-

freq (cm^{-1}) (corr)[a]		symmetry D_{8h} ➡	correlations D_{4h}	D_{2d}
180		e_{2u}	$b_{1u} \oplus b_{2u}$	$a_1 \oplus a_2$
316 (270)[b]	ν_{17}[c]	e_{2g}	$b_{1g} \oplus b_{2g}$[c]	$b_1 \oplus b_2$[c]
597		b_{1u}	a_{1u}	b_1
710 (720)[b]	ν_1[d]	a_{1g}	a_{1g}[d]	a_1
726		b_{1u}	a_{1u}	b_1
860		e_{2u}	$b_{1u} \oplus b_{2u}$	$a_1 \oplus a_2$
966		b_{2g}	a_{2g}	a_2
1131		e_{2g}	$b_{1g} \oplus b_{2g}$	$b_1 \oplus b_2$
1141 (1120)[e]		b_{1g}[e]	a_{1g}	a_1
1296 (1600)[b]	ν_2[d]	b_{1g}	a_{1g}[d]	a_1[d]
1504		e_{2g}	$b_{1g} \oplus b_{2g}$	$b_1 \oplus b_2$
2857		b_{2g}	a_{2g}	a_2
2927		a_{1g}	a_{1g}	a_1

[a] *Ab initio* frequencies (HF/6-31G) multiplied by 0.89, the standard correction with Gaussian-90. Geometry-optimized (HF/6-31G) bond lengths used: C–C, 1.403 Å; C–H, 1.083 Å. Important modes are depicted in Figures 6 and 7. [b] Observed in this work. [c] Jahn–Teller active in the excited state—see Figure 3. [d] Forms excited state totally symmetric progression—see Figure 3. [e] Reported by Dvorak and Michl[17] and assigned by us as the ground state Jahn–Teller active mode—see text.

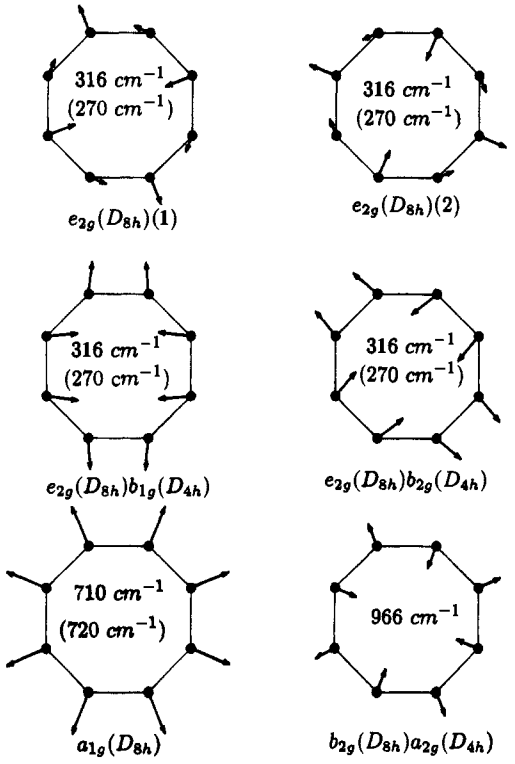

Figure 6. Some normal modes (carbon atoms only) and frequencies obtained from the Gaussian-90 calculation with corresponding experimentally assigned values in parentheses and obtained as explained in the text and Table 2. The middle pair of modes are the sum ($b_{2g}(D_{4h})$) and difference ($b_{1g}(D_{4h})$) of the pair above and belong to the indicated D_4 irreps with our conventions and definitions.

summarized in Table 2 for modes of interest, and the mostimportant are also depicted in Figures 6 and 7 using the Gaussian-90 relative displacements.

The first thing that becomes strikingly clear is that there is no possibility of accounting for the observed totally symmetric vibration at 1600 cm^{-1} on the basis of D_{8h} symmetry. Of the two possible a_{1g} frequencies, experiment and theory correlate nicely for the lower one (720 *vs* 710 cm^{-1} for the C–C stretch, Table 2), but the higher one (C–H stretch) is predicted at a frequency around 2900 cm^{-1} for D_{8h} COT^-. Furthermore, only b_{1g} and b_{2g} modes are Jahn–Teller active in the $^2E_{2u}(D_{8h})$ ground state of COT^- since the symmetric product $[E^2_{2u}] = a_{1g} \oplus b_{1g} \oplus b_{2g}$. And all of these modes are calculated (Table 2) to be very far from the observed (~270 cm^{-1}) Jahn–Teller mode. On the other hand, the temperature dependence of the MCD tells us that we must be within the dynamic range of D_{8h} symmetry (since any lower symmetry requires a temperature-independent MCD), and the much reduced (from the theoretical value) ground state orbital angular momentum strongly suggests a dynamic Jahn–Teller effect in the ground state. We shall argue in the remainder of this paper that all of these facts can be accounted for if we assume that the excited electronic state has D_{4h} (or D_{2d}) symmetry. The 270 cm^{-1} mode is then associated with a Jahn–Teller effect *in the excited state*, and the ground state properties of COT^- are accounted for by a combination of Jahn–Teller, spin–orbit, and crystal field effects.

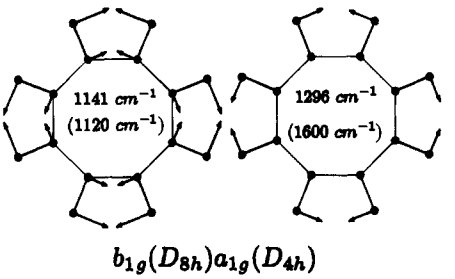

Figure 7. The b_{1g} normal modes and frequencies obtained from the Gaussian-90 calculation with experimentally assigned values in parentheses. The right-hand mode is responsible for the 1600 cm^{-1} totally symmetric progression observed in the excited electronic state. Each carbon-atom motion in that mode is exactly opposed to the corresponding hydrogen-atom motion but with ≤~10% the amplitude. The displacements are too small to be seen to the scale of the figure. These two b_{1g} modes are probably significantly mixed in the excited electronic state in view of the substantially higher value required for the higher frequency mode (1600 cm^{-1}).

3. The Molecular Hamiltonian.

We follow the general approach of Piepho[27] and write the total molecular Hamiltonian as

$$\hat{H}_T(r, Q) = \hat{H}_{el}(r, Q) + \hat{T}_N(Q) \tag{5}$$

where $\hat{T}_N$ is the nuclear kinetic energy operator, r and Q symbolize all electronic and nuclear coordinates, respectively, and $\hat{H}_{el}$ inlcudes all Coulombic interactions as well as the electronic kinetic energy terms.

The relevant electronic transition, $^2E_{2u}(D_{8h}) \rightarrow {}^2E_{1g}(D_{8h})^2E_g(D_{4h}) \equiv {}^2E_g$ or $^2E_{2u}(D_{8h}) \rightarrow {}^2E_{1g}(D_{8h})^2E(D_{2d}) \equiv {}^2E$, is between orbitally degenerate electronic states. The chain notation, $^2E_{1g}(D_{8h})^2E_g(D_{4h})$, shows the D_{8h} parentage of the D_{4h} state, etc. Hereafter, we rather arbitrarily designate the excited state as ^2E_g to avoid continually writing "$^2E_g(D_{4h})$ or $^2E(D_{2d})$". *Thus any statement about the D_{4h} excited state will imply a corresponding statement in D_{2d} which we generally do not explicitly elaborate.* Our data do not permit a clear-cut choice between these two possible excited state symmetries. We designate molecular orbitals (MOs) as $|e_n \pm n\rangle$ with $n = 1$ ($e_{1g}(e_g)$) or 2 (e_{2u}), and these MOs transform as the standard basis functions defined in Table 1. These MOs satisfy eq 6 at $Q = 0$:

$$\hat{H}^0_{el}|e_n \pm n\rangle^0 = W^0_n|e_n \pm n\rangle^0; \quad n = 1, 2 \tag{6}$$

and we make the usual assumption that the MOs are not a function of Q, i.e., $|e_n \pm n\rangle = |e_n \pm n\rangle^0$. (Correlations of some of the irreps of D_{8h} with those of D_{4h} and D_{2d} are shown in the last column of Table 1 and the last two columns of Table 2.)

(27) Piepho, S. B. *J. Am. Chem. Soc.* **1988**, *110*, 6319–6326.

We now permit nuclear displacements by expanding $\hat{H}_{el}$ in a Taylor's series through quadratic terms:

$$\hat{H}_{el}(r, Q) = \hat{H}^0_{el}(r, Q) + \sum_{\eta} l_\eta Q_\eta + \frac{1}{2}\sum_{\eta\mu} k_{\eta\mu} Q_\eta Q_\mu \quad (7)$$

Considering the electronic ground state first, we distinguish between Jahn–Teller-active and non-Jahn–Teller-active modes. For the latter, we can (and do) set all the l_η and quadratic cross terms equal to zero. However, for the former, we cannot arbitrarily *choose* the $l_\eta = 0$; the non-zero l_η produce first-order JT effects. We do, however, eliminate the $Q_\alpha Q_\beta$ cross terms by assuming that second-order JT effects are negligible.

For the excited electronic state, an expression analogous to eq 7 applies with $\hat{H}^0_{el}$ augmented by a constant term, W_0, corresponding to the energy difference between the two states. The l_η can be different from zero for both totally symmetric and Jahn–Teller modes. In addition, we cannot necessarily eliminate the $Q_\alpha Q_\beta$ cross terms. We *assume* in our treatment that all such terms are negligible.

4. Excited State Jahn–Teller Effect. In D_{8h} symmetry, the only Jahn–Teller-active modes in the $^2E_{1g}$ excited state are of symmetry e_{2g} since the symmetric product of E_{1g} gives $[E^2_{1g}] = a_{1g} \oplus e_{2g}$. When we lower the symmetry to D_{4h} (to account for the appearance of the 1600 cm^{-1} totally symmetric mode), $^2E_{1g}(D_{8h}) \rightarrow {}^2E_g(D_{4h})$ and $e_{2g}(D_{8h}) \rightarrow b_{1g}(D_{4h}) \oplus b_{2g}(D_{4h})$ (Table 2), both of these latter modes now being Jahn–Teller-active. Indeed, the *ab initio* calculation (Table 2) predicts a D_{8h} e_{2g} mode quite close (316 cm^{-1}) to the observed 270 cm^{-1} Jahn–Teller frequency. We identify the 1600 cm^{-1} mode with the higher of the two $b_{1g}(D_{8h})a_{1g}(D_{4h})$ modes (Figure 7), which is calculated to be at 1296 cm^{-1} (Table 2). This frequency is about 300 cm^{-1} lower than observed, but we note that the two $b_{1g}(D_{8h})a_{1g}(D_{4h})$ frequencies are calculated to be within about 150 cm^{-1} of each other. Thus the calculated frequencies of these excited state modes will be especially sensitive to inadequacies in the *ab initio* calculation which in any event is for the ground (D_{8h}) electronic state of COT^-. (Note that with the conventions of Table 1, $b_{1g}(D_{8h})$ is the totally antisymmetric in-plane *C–C stretch* and $b_{2g}(D_{8h})$ (Figure 6) is the corresponding in-plane *bend*. We also once more emphasize that $b_{1g}(D_{4h})$ means $b_{1g}(D_{4h})$ or $b_1(D_{2d})$, etc.)

We now make the simplest assumption, namely that there is a single Jahn–Teller-active mode in the $^2E_g(D_{4h})$ excited state, and we identify it as one of the (in D_{4h}) distinct partners of $e_{2g}(D_{8h})$, *i.e.* $b_{1g}(D_{4h})$ or $b_{2g}(D_{4h})$. These two modes are shown in the middle panel of Figure 6. The formal solution of the problem is identical for either,[20] and we arbitrarily choose $e_{2g}(D_{8h})b_{1g}(D_{4h})$. We also assume that the ground state vibronic functions are simple Born–Oppenheimer products. (We remove this restriction later.) Finally, we note that the $E_g \otimes b_{1g}(D_{4h})$ and $E_{2u} \otimes b_{1g}(D_{8h})$ Jahn–Teller problems are formally identical, a fact that may be confirmed by inspecting the coupling coefficients and correlations in Tables 1 and 3. Thus the following analysis is equally applicable when we later consider the ground state Jahn–Teller effect.

We first transform to the dimensionless variables,

$$q_\alpha \equiv \hbar^{-1}(h\nu_\alpha)^{1/2} Q_\alpha$$

$$\lambda_\alpha \equiv \hbar(h\nu_\alpha)^{-3/2} l_\alpha \quad (8)$$

where $\nu_\alpha = (2\pi)^{-1}\sqrt{k}$ is the fundamental vibrational frequency associated with normal coordinate Q_α. Using these definitions and the previous assumptions, eq 7 becomes

Table 3. Selected Vector Coupling Coefficients in Point Group D_8 in the Style of Griffith[33]

	E_n			E_m			E_m	
$A_2 \otimes E_n$	$+n$	$-n$	$B_1 \otimes E_n$	$+m$	$-m$	$B_2 \otimes E_n$	$+m$	$-m$
$\|a_2\rangle\|+n\rangle$	+1	0	$\|b_1\rangle\|+n\rangle$	0	+1	$\|b_2\rangle\|+n\rangle$	0	−1
$\|a_2\rangle\|-n\rangle$	0	−1	$\|b_1\rangle\|-n\rangle$	+1	0	$\|b_2\rangle\|-n\rangle$	+1	0
$n = 1, 2, 3$			$n, m = 1, 3; 2, 2; 3, 1$			$n, m = 1, 3; 2, 2; 3, 1$		

			E_2	
$E_1 \otimes E_1$	$A_1\ a_1$	$A_2\ a_2$	$+2$	-2
$\|+1\rangle\|+1\rangle$	0	0	1	0
$\|+1\rangle\|-1\rangle$	$2^{-1/2}$	$2^{-1/2}$	0	0
$\|-1\rangle\|+1\rangle$	$2^{-1/2}$	$-2^{-1/2}$	0	0
$\|-1\rangle\|-1\rangle$	0	0	0	1

			E_2	
$E_3 \otimes E_3$	$A_1\ a_1$	$A_2\ a_2$	$+2$	-2
$\|+3\rangle\|+3\rangle$	0	0	0	1
$\|+3\rangle\|-3\rangle$	$2^{-1/2}$	$2^{-1/2}$	0	0
$\|-3\rangle\|+3\rangle$	$2^{-1/2}$	$-2^{-1/2}$	0	0
$\|-3\rangle\|-3\rangle$	0	0	1	0

			E_2	
$E_1 \otimes E_3$	$B_1\ b_1$	$B_2\ b_2$	$+2$	-2
$\|+1\rangle\|+3\rangle$	$2^{-1/2}$	$-2^{-1/2}$	0	0
$\|+1\rangle\|-3\rangle$	0	0	0	1
$\|-1\rangle\|+3\rangle$	0	0	1	0
$\|-1\rangle\|-3\rangle$	$2^{-1/2}$	$2^{-1/2}$	0	0

	E_1		E_3	
$E_1 \otimes E_2$	$+1$	-1	$+3$	-3
$\|+1\rangle\|+2\rangle$	0	0	1	0
$\|+1\rangle\|-2\rangle$	0	1	0	0
$\|-1\rangle\|+2\rangle$	1	0	0	0
$\|-1\rangle\|-2\rangle$	0	0	0	1

	E_1		E_3	
$E_2 \otimes E_3$	$+1$	-1	$+3$	-3
$\|+2\rangle\|+3\rangle$	0	0	0	1
$\|+2\rangle\|-3\rangle$	0	1	0	0
$\|-2\rangle\|+3\rangle$	1	0	0	0
$\|-2\rangle\|-3\rangle$	0	0	1	0

$E_2 \otimes E_2$	$A_1\ a_1$	$A_2\ a_2$	$B_1\ b_1$	$B_2\ b_2$
$\|+2\rangle\|+2\rangle$	0	0	$2^{-1/2}$	$-2^{-1/2}$
$\|+2\rangle\|-2\rangle$	$2^{-1/2}$	$2^{-1/2}$	0	0
$\|-2\rangle\|+2\rangle$	$2^{-1/2}$	$-2^{-1/2}$	0	0
$\|-2\rangle\|-2\rangle$	0	0	$2^{-1/2}$	$2^{-1/2}$

$$\hat{H}_{el} = \hat{H}^0_{el} + \lambda_{b_{1g}} q_{b_{1g}} h\nu_{b_{1g}} + \frac{1}{2}\sum_\alpha q^2_\alpha h\nu_\alpha \quad (9)$$

The sum runs over all $3N - 6$ normal coordinates of the molecule.

We seek solutions of the dynamic problem,

$$\hat{H}_T \Psi^{ex} = E^{ex}\Psi^{ex} \quad (10)$$

and write Ψ^{ex} in the non-adiabatic form,

$$\Psi^{ex} = |^2E_1 1(^2E1)\rangle|\chi_1(q)\rangle + |^2E_1 - 1(^2E - 1)\rangle\,|\chi_{-1}(q)\rangle \quad (11)$$

where the $|\chi_{\pm1}(q)\rangle$ are unknown functions of q which must be determined. (Hereafter we generally omit the D_{8h} parentage of D_{4h} functions so that for example $|E_1 1(E1)\rangle$ is simply written $|E1\rangle$, etc., and we usually omit u and g subscripts; E_1 and E are always understood to be g and $E2$ is always u.) It is well-known that an analytic solution of this problem is possible if

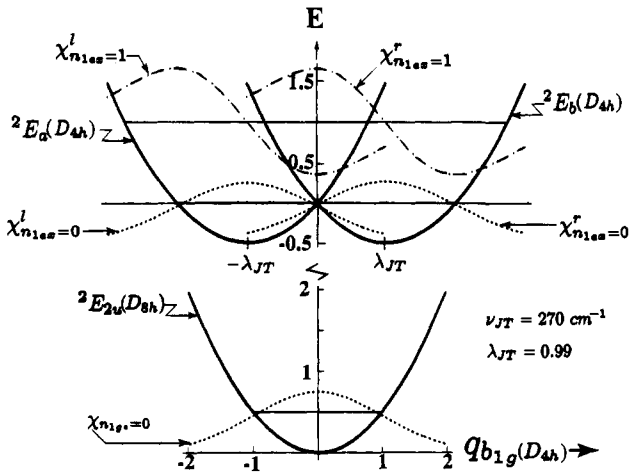

Figure 8. Potential surfaces and associated oscillator functions for the excited state Jahn–Teller effect. $q_{b_{1g}}(D_{4h})$ (or $q_{b_{2g}}(D_{4h})$) is a component of $q_{e_{2g}}(D_{8h})$ which becomes Jahn–Teller active when the excited electronic state equilibrium point group symmetry is reduced to D_{4h}—see text. Energy is in units of $h\nu_{JT}$ with ν_{JT} = 270 cm^{-1}, and $\lambda_{b_{1g}} = \lambda_{JT} = 0.99$.

we make the following transformation of electronic basis:

$$|^2E_a\rangle = 2^{-1/2}(|^2E1\rangle + |^2E-1\rangle); \quad |^2E_b\rangle = 2^{-1/2}(|^2E1\rangle - |^2E-1\rangle) \quad (12)$$

If we now write

$$\Psi^{ex} = |^2E_a\rangle|\chi_a(q)\rangle + |^2E_b\rangle|\chi_b(q)\rangle \quad (13)$$

we can easily demonstrate that the solutions to eq 10 are

$$\Psi^{ex}_a = |^2E_a\rangle|\chi^l_{ex}(q)\rangle; \quad \Psi^{ex}_b = |^2E_b\rangle|\chi^r_{ex}(q)\rangle \quad (14)$$

where the $\chi^l_{ex}(q)$ and $\chi^r_{ex}(q)$ are *harmonic oscillator functions* displaced respectively to the left or to the right by $\lambda_{b_{1g}}$ from $q_{b_{1g}} = 0$ (Figure 8). This is so because

$$\left(T_N + \frac{1}{2}q^2_{b_{1g}}h\nu_{b_{1g}} \pm \lambda_{b_{1g}}q_{b_{1g}}h\nu_{b_{1g}}\right)\left|\chi^{l,r}_{ex}(q)\right\rangle = \left(n_{b_{1g}} + \frac{1}{2} - \frac{1}{2}\lambda^2\right)h\nu_{b_{1g}}\left|\chi^{l,r}_{ex}(q)\right\rangle \quad (15)$$

Thus in the absence of external perturbations, each vibronic level of the ^2E_g excited state is doubly degenerate. The potential surfaces obtained by diagonalizing $\hat{H}_{el}$ are shown in Figure 8.

To calculate the absorption and MCD spectrum, we must calculate the transition probabilities between the ground and excited electronic states. Since our data are applicable for very low temperatures, we assume that only the zero-point vibrational level of the ground electronic state is populated. Assuming that the ground state ($^2E_{2u}$) vibronic wave functions are simple Born–Oppenheimer products, we write

$$\Psi^{gs}_{\pm} = |^2E_2 \pm 2\rangle|\chi_{gs}(q)\rangle \quad (16)$$

where $|^2E_2 \pm 2\rangle$ and only a single set of (undisplaced) oscillators is required since we have assumed for the moment that all ground state JT effects are negligible. The electric dipole operator has components $m_{E_{1u}\pm1}$, $m_{A_{2u}}$ in point group D_{8h}, and the only nonzero transition moments are therefore (Tables 1 and 3)

$$\langle E_2 2|E_1 1|E_1 1(E1)\rangle = \langle E_2 - 2|E_1 - 1|E_1 - 1(E-1)\rangle \quad (17)$$

The Franck–Condon (FC) vibrational overlap factors are determined from

$$\langle\chi^{l,r}_{ex}(q)|\chi_{gs}(q)\rangle = \langle\chi^{l,r}_{ex}(q)|\chi_{n_{gs}=0}(q)\rangle \quad (18)$$

We make the harmonic approximation and assume that the fundamental vibrational frequencies do not change much between the ground and excited electronic states, an assumption supported by the COT^- emission spectra.[17] It then follows that the excited state vibrational quantum numbers can change only for the totally symmetric vibrations *and* for the JT-active mode (because of the $\pm\lambda_{b_{1g}}$ displacements of the excited state potential minima—Figure 8).

To account for the experimental data, we must develop theoretical expressions for the absorption and MCD. Clearly the Born–Oppenheimer assumption is invalid and the expressions in Section IV.1 are not applicable. We therefore derive explicit expressions for the absorption and MCD of the individual vibronic transitions comprising the band. The band contours then reflect appropriate sums over all such transitions.

Because of the simplicity of the solution of the Jahn–Teller problem (eq 14), we may proceed in close analogy to the Born–Oppenheimer, Rigid-Shift case. Transitions are from an *electronically* doubly degenerate ground state (eq 16) to a *vibronically* doubly degenerate excited state (eq 14). Since the MCD is strongly temperature dependent, we will for the moment only consider $\mathcal{C}$ terms. We may then use eqs 1 and 2 if we identify $|J\lambda\rangle$, $|J\lambda'\rangle$ with the *vibronic* functions of eq 14. In addition, we include two excited state totally symmetric modes, i.e., we assume that the excited electronic state is displaced (with respect to the ground electronic state) along the 720 cm^{-1} $a_{1g}(D_{8h})$ coordinate (Figure 6) and along the 1600 cm^{-1} $b_{1g}(D_{8h})a_{1g}(D_{4h})$ coordinate (Figure 7). *It is the latter displacement which in part (see later) lowers the excited state equilibrium point group symmetry from D_{8h} to D_{4h} (or D_{2d}).*

Using the vector coupling coefficients of Table 3, we obtain for each vibronic line,

$$\bar{\mathcal{C}}_0(n_1n_2n_3) = \frac{|m|^2}{3}\bar{L}_Z\langle\chi^l_{ex}|\chi_{gs}\rangle_{n_1n_2n_3}\langle\chi^r_{ex}|\chi_{gs}\rangle_{n_1n_2n_3} \quad (19)$$

$$\bar{\mathcal{D}}_0(n_1n_2n_3) = \frac{|m|^2}{6}(|\langle\chi^l_{ex}|\chi_{gs}\rangle_{n_1n_2n_3}|^2 + |\langle\chi^r_{ex}|\chi_{gs}\rangle_{n_1n_2n_3}|^2) = \frac{|m|^2}{3}|\langle\chi^l_{ex}|\chi_{gs}\rangle_{n_1n_2n_3}|^2 \quad (20)$$

with

$$\langle\chi^{l,r}_{ex}|\chi_{gs}\rangle_{n_1n_2n_3} \equiv \langle\chi^{l,r}_{n_{1ex}}(q_1)|\chi_{n_{1gs}=0}(q_1)\rangle\langle\chi_{n_{2ex}}(q_2)|\chi_{n_{2gs}=0}(q_2)\rangle\langle\chi_{n_{3ex}}(q_3)|\chi_{n_{3gs}=0}(q_3)\rangle$$

where q_1, q_2, q_3 designate respectively the Jahn–Teller active and two totally symmetric modes. $\bar{L}_Z$ is the ground state orbital angular momentum as defined in eq 3, and m is a reduced transition moment matrix element which cancels from $\bar{\mathcal{C}}_0/\bar{\mathcal{D}}_0$ ratios. The very last relation in eq 20 results because $|\langle\chi^1_{ex}|\chi_{gs}\rangle_{n_1n_2n_3}|^2 = |\langle\chi^r_{ex}|\chi_{gs}\rangle_{n_1n_2n_3}|^2$ by symmetry.

The calculated MCD and absorption band contours are obtained by substituting in eq 1 for $\bar{\mathcal{C}}_0$ and $\bar{\mathcal{D}}_0$ the respective

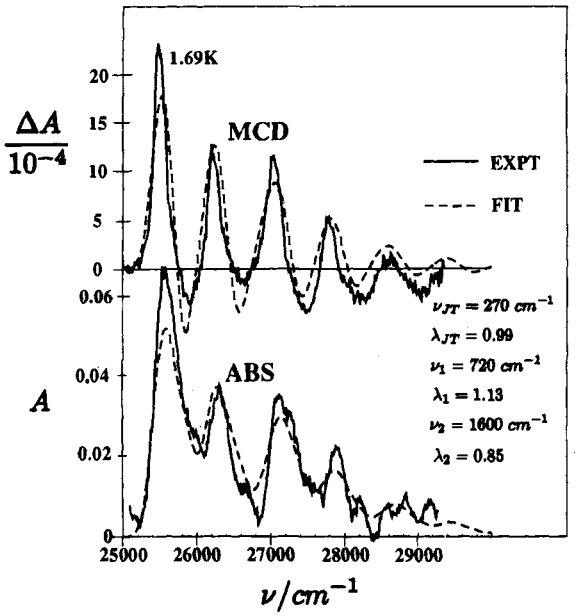

Figure 9. "Best fit" (dashed curves) of the experimental absorption and lowest temperature MCD spectra (solid curves) and resulting parameters.

values

$$\bar{\mathcal{C}}_0 = \sum_{n_1n_2n_3} \bar{\mathcal{C}}_0(n_1n_2n_3) f_{n_1n_2n_3}(\mathcal{E})$$

$$\bar{\mathcal{D}}_0 = \sum_{n_1n_2n_3} \bar{\mathcal{D}}_0(n_1n_2n_3) f_{n_1n_2n_3}(\mathcal{E}) \qquad (21)$$

where $f_{n_1n_2n_3}(\mathcal{E})$ is a normalized *ad hoc* line shape function which we choose to be Gaussian, and we are presently assuming that $\bar{\mathcal{A}}_1 = \bar{\mathcal{B}}_0 = 0$. We can understand why the MCD sign alternates in the Jahn–Teller mode progression but not in the totally symmetric ones by examining the Franck–Condon product on the right side of eq 19. This factor is clearly positive for a totally symmetric progression but involves the product $\langle\chi^l_{n_{1ex}}(q_1)|\chi_{n_{1gs}=0}(q_1)\rangle\langle\chi^r_{n_{1ex}}(q_1)|\chi_{n_{1gs}=0}(q_1)\rangle$ for the Jahn–Teller progression. The latter changes sign for each successive value of n_{1ex}, since the excited state surfaces are displaced in opposite directions along the Jahn–Teller coordinate, as illustrated in Fiture 8 where the first two excited state vibrational functions are shown.

The parameters to be fit to experiment are W_0 and the values of ν_i and λ_i for each mode. Once the λ_i are specified, the Franck–Condon factors are completely defined and are easily evaluated by a well-known formula involving the associated Laguerre polynomials.[28] We note that it is also possible to do this calculation using a basis of undisplaced harmonic oscillators, and in fact we have done this by a slight modification of a program previously used by one of us in mixed-valence calculations.[27] Identical results were obtained by both procedures.

We have done the fitting by trial and error, and our best fit criterion is simply visual inspection. The fit is shown in Figure 9, along with the resulting parameters, for the lowest-temperature MCD spectrum and the averaged absorption spectrum. The fits are quite good; the observed vibronic features are well accounted for. Detailed vibronic assignments are shown by the stick spectra in Figure 3. The Jahn–Teller energy associated with the 270 cm^{-1} mode is,

$$E_{JT} = {}^1/_2\lambda^2_{JT}h\nu_{JT} = 132\ cm^{-1} \qquad (22)$$

which happens to be almost exactly the zero-point energy of the mode. Since there are perturbations which split the vibronic degeneracy (see subsection 5 immediately below), the molecule readily oscillates between the two excited state potential minima of Figure 8.

5. The Electronic Ground State of COT^-. Having obtained a reasonable fit of the absorption and MCD spectra, we must now consider the quantitative properties of the electronic ground state of COT^-. In particular, we have noted earlier (Section IV.1) that the ground state orbital angular momentum is very much smaller than the theoretical value, which implies a strong quenching and thus a large ground state Jahn–Teller effect. Furthermore, the MCD will be extremely sensitive to any effects which split the degeneracy of the ground state manifold since the MCD is dominated by population effects ($\mathcal{C}$ terms). Two obvious sources of such splittings are spin–orbit and crystal field (low site-symmetry) interactions. We now show that both of these effects, in addition to Jahn–Teller coupling, are required to account quantitatively for the magnitude and temperature dependence of the MCD.

(a) Spin–Orbit Coupling and the Jahn–Teller Effect. We must take explicit account of spin–orbit coupling since $\zeta \approx 32$ cm^{-1} for the carbon 2p orbital.[29] While an effect of this magnitude can be neglected in the excited state since our line widths are on the order of $\approx$200 cm^{-1}, this is by no means the case in the ground state where any effect on the order of or greater than kT can drastically alter the calculated MCD. We choose ground state vibronic functions that are diagonal in the Jahn–Teller effect. In point group D_{8h}, the possible Jahn–Teller-active modes in the $^2E_{2u}$ ground state are b_{1g} or b_{2g}. The two obvious candidates from the *ab initio* calculation are (Table 2) $\nu_{b_{2g}} = 966$ cm^{-1} (Figure 6) or $\nu_{b_{1g}} = 1141$ cm^{-1} (Figure 7). The higher energy b_{1g} mode, which is dominated by H-atom motions (Figure 7), is excluded because it has already been identified with the totally symmetric (in D_{4h}) mode at 1600 cm^{-1} (whose MCD progression does *not* alternate in sign). Also, the higher energy b_{2g} mode calculated at 2857 cm^{-1} is far too high to be relevant since it is almost entirely an H-atom stretching motion. There are strong theoretical arguments[20,21] for preferring the antisymmetric ring stretching mode, and we therefore choose the 1141 cm^{-1} b_{1g} mode (Figure 7) as our Jahn–Teller-active mode. (We comment further on this choice below.) As noted before, the Jahn–Teller treatment for $E_{2u} \otimes b_{1g}$ in D_{8h} is formally identical to the $E_g \otimes b_{1g}$ treatment in D_{4h} presented earlier. Our four ground state electronic basis functions are given by,

$$\phi^{\pm}_{\pm} = 2^{-1/2}(|^2E_2 \pm {}^1/_2 2\rangle \pm |^2E_2 \pm {}^1/_2 - 2\rangle) \qquad (23)$$

where the superscript on ϕ designates spin, and the subscript designates the sign between the two $|^2E_2\rangle$ kets. The corresponding four vibronic functions are,

$$\Psi^+_+ = \phi^+_+\chi^l_0; \quad \Psi^+_- = \phi^+_-\chi^r_0; \quad \Psi^-_+ = \phi^-_+\chi^l_0; \quad \Psi^-_- = \phi^-_-\chi^r_0 \qquad (24)$$

where the subscript zeros indicate the $n = 0$ vibrational level—the only one occupied because of the low temperature. The sub- and superscripts on Ψ are defined as in eq 23 and the superscripts on χ are defined by the ground state analog of eq 15.

(28) Fulton, R. L.; Gouterman, M. *J. Chem. Phys.* **1961**, *35*, 1059.

Table 4. Matrix of $(\hat{H}_{JT} + \hat{H}_{SO} + \hat{H}_{CF})$ in the Vibronic Jahn–Teller Basis

	Ψ_+^+	Ψ_-^+	Ψ_+^-	Ψ_-^-
Ψ_+^+	$^1/_2h\nu(1-\lambda^2_{JT})+\Delta/2$	$-\zeta\bar{L}_z\gamma_{00}/2$		
Ψ_-^+	$-\zeta\bar{L}_z\gamma_{00}/2$	$^1/_2h\nu(1-\lambda^2_{JT})-\Delta/2$		
Ψ_+^-			$^1/_2h\nu(1-\lambda^2_{JT})+\Delta/2$	$+\zeta\bar{L}_z\gamma_{00}/2$
Ψ_-^-			$+\zeta\bar{L}_z\gamma_{00}/2$	$^1/_2h\nu(1-\lambda^2_{JT})-\Delta/2$

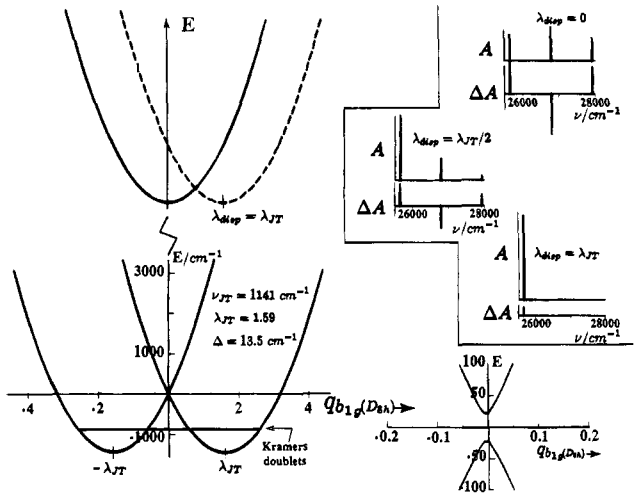

Figure 10. Potential surfaces for the ground state Jahn–Teller effect. The ground state point group symmetry is D_{8h}. Energy is in cm^{-1} with $\nu_{JT} = 1141\ cm^{-1}$; $\lambda_{JT} = 1.59$, crystal field $\Delta = 13.5\ cm^{-1}$. The upper right inset shows MCD and absorption stick spectra of the Jahn–Teller progression predicted for the case where the upper potential surface (solid parabola) minimum is at $q_{b_{1g}} = 0$ (top of inset), for the case where the upper potential surface (dashed parabola) minimum coincides with $q_{b_{1g}} = \lambda_{b_{1g}} = \lambda_{JT}$ (bottom of inset), and where the upper potential surface minimum (not shown) coincides with $q_{b_{1g}} = {}^1/_2\lambda_{b_{1g}} = {}^1/_2\lambda_{JT}$ (middle of inset). The location of the two populated Kramers doublets which are split by $W = [(\zeta\bar{L}_z\gamma_{00})^2 + \Delta^2]^{1/2}$ is shown by horizontal bars. The splitting ($W = 13.9\ cm^{-1}$) is unresolved to the scale of the figure. The lower right corner shows a blowup of the avoided crossing which arises due to spin–orbit coupling.

To take account of spin–orbit coupling, we add to our Hamiltonian the term,

$$\hat{H}_{SO} = \sum_i \xi(r_i)\mathbf{l}(i)\cdot\mathbf{s}(i) \tag{25}$$

where l and s are the one-electron orbital and spin angular momentum operators. For a carbon 2p orbital, ζ_{2p_C}, the expectation value of $\xi(r)$ over the radial wave function is assigned the value 32 cm^{-1}.[29] The matrix of $(\hat{H}_{SO} + \hat{H}_{JT}) + \hat{H}_{CF}$ (considered later) in the basis of eq 24 is given in Table 4. Diagonalization of this matrix produces two Kramers doublets which are separated in energy by $\zeta\bar{L}_z\gamma_{00}$, where $\bar{L}_z$ is defined in eq 3 and $\gamma_{00} = e^{-\lambda^2_{JT}} = \langle\chi^l_{n_{gs}=0}(q_{b_{1g}})|\chi^r_{n_{gs}=0}(q_{b_{1g}})\rangle$ is the Ham-effect quenching factor—see Figure 10. The corresponding eigenfunctions are of the form,

$$\Phi_1 = c_1\Psi_+^+ + c_2\Psi_-^+; \quad \Phi_2 = c_1\Psi_+^- - c_2\Psi_-^-$$

$$\Phi_3 = c_2\Psi_+^+ - c_1\Psi_-^+; \quad \Phi_4 = c_2\Psi_+^- + c_1\Psi_-^-; \tag{26}$$

where subscripts 1, 2 designate the lower-energy doublet and 3, 4 the higher-energy doublet. Furthermore, in the absence of a crystal field, one finds that $c_1 = c_2 = 2^{-1/2}$. The potential surfaces, obtained by diagonalizing $\hat{H}_{el}$ in the $\phi^{\pm}_{\pm}$ basis, are shown in Figure 10. (In obtaining eq 26, we have neglected matrix elements of the form $\langle\phi^{\pm}_{\pm}\chi_0|\hat{H}_{SO}|\phi^{\pm}_{\pm}\chi_n\rangle$ ($n > 0$). Such elements would be of the form $\zeta\bar{L}_z\gamma_{0n}/\Delta E$, where ΔE is a vibrational spacing (~1000 cm^{-1}) and hence would be very small.)

We must now recalculate the MCD and absorption spectra to compare with experiment. The excited state is unchanged, but the ground electronic state has altered drastically (Figure 10). The double electronic degeneracy has changed to a double vibronic degeneracy as a result of the Jahn–Teller coupling, and that degeneracy in turn has been split by the spin–orbit coupling into two Kramers doublets separated in energy by $\zeta\bar{L}_z\gamma_{00}$. Equation 21 is still applicable, but both Kramers doublets, weighted by appropriate population factors, will contribute to the absorption and MCD if their separation is not $\gg kT$. Furthermore, we must consider possible $\mathcal{B}$-term contributions due to field induced mixing of the two Kramers doublets. Using the coupling coefficients in Table 3 we find that $\mathcal{B}$-term contributions are in fact zero in this case and,

$$\bar{\mathcal{C}}_0^{(1,2)} = \frac{|m|^2}{3}\langle\chi_0^l|\chi_{ex}\rangle_n\langle\chi_0^r|\chi_{ex}\rangle_n(\gamma_{00}\bar{L}_Z + 1)$$

$$\bar{\mathcal{C}}_0^{(3,4)} = \frac{|m|^2}{3}\langle\chi_0^l|\chi_{ex}\rangle_n\langle\chi_0^r|\chi_{ex}\rangle_n(\gamma_{00}\bar{L}_Z - 1) \tag{27}$$

$$\bar{\mathcal{D}}_0^{(1,2)} = \bar{\mathcal{D}}_0^{(3,4)} = \frac{|m|^2}{6}(|\langle\chi_0^l|\chi_{ex}\rangle_n|^2 + |\langle\chi_0^r|\chi_{ex}\rangle_n|^2) \tag{28}$$

where in $\langle\chi_0^{l,r}|\chi_{ex}\rangle_n$ the subscript zero means that all vibrational quantum numbers in the ground electronic state are zero, and the subscript n symbolizes all relevant excited state vibrational quantum numbers. Superscripts (1, 2) and (3, 4) designate respectively the lower and upper Kramers doublets.

We note that unlike the earlier treatment (eqs 16–21), there is no requirement that $|\langle\chi_0^l|\chi_{ex}\rangle_n|^2 = |\langle\chi_0^r|\chi_{ex}\rangle_n|^2$, because the ground and excited states belong to different point groups, and thus the ground state minimum along the $b_{1g}(D_{8h})$ Jahn–Teller coordinate (before ground state Jahn–Teller coupling is turned on) need not coincide with the excited state minimum. Indeed if it did, we would expect to see a Jahn–Teller progression in the MCD and absorption spectra (after turning on the Jahn–Teller effect) corresponding to the 1141 cm^{-1} mode. As the excited electronic state potential surface is displaced along $q_{b_{1g}}(D_{8h})$, this progression becomes steadily shorter, and when the upper surface minimum is directly over either of the ground state potential minima (for example dashed upper surface, Figure 10), all the intensity is in the no-phonon line. Calculated absorption and MCD stick spectra in the ground state Jahn–Teller mode are shown in the upper right panel of Figure 10 for the solid ($\lambda_{disp} = 0$) and dashed ($\lambda_{disp} = \lambda_{JT}$) excited state potential surfaces and for one half-way in between ($\lambda_{disp} = \lambda_{JT}/2$), to illustrate this effect. Note that $\lambda_{disp} \neq 0$ means that the excited state distortion from D_{8h} to D_{4h} symmetry is now along both $b_{1g}(D_{8h})a_{1g}(D_{4h})$ coordinates of Figure 7. These distortions are the result of a higher order (but not small) effect since $b_{1g}(D_{8h})$ is not Jahn–Teller active in the excited $^2E_{1g}$ electronic state.

Assuming that the upper potential surface is in the rough vicinity of the dashed curve ($\lambda_{disp} \approx \lambda_{JT}$, Figure 10), the only

(29) Kayama, K.; Baird, J. C. *J. Chem. Phys.* **1967**, *46*, 2604.

change in the calculated MCD and absorption band contours (Figure 9) would arise from the spin−orbit interaction in the ground state, each of the two Kramers doublets producing population-weighted identical spectral features separated by the ground state spin−orbit splitting of $\zeta\bar{L}_Z\gamma_{00}$. In the present case, using $\zeta = 32$ cm^{-1}, $\bar{L}_Z = 1.33$, and $\lambda_{JT} = 1.83$ (see below), this splitting is calculated to be 1.5 cm^{-1}. Since excited state line widths are $\geq$200 cm^{-1}, our previous fit (Figure 9) is not appreciably changed. Recall that the applicable surfaces for the fit are the ones shown in Figure 8, which involves an *entirely different* b_{1g} mode than that in Figure 10. The former is a D_{4h} b_{1g} mode whose parentage was a D_{8h} e_{2g} mode (Figure 6). The latter is a D_{8h} b_{1g} mode (Figure 7).

We now calculate the theoretical zeroth moment ratio M_0/A_0 (eq 4) to compare with experiment (Figure 5). Working with the zeroth moments has very important advantages. First, it permits us to average over the spectral noise. But, much more important, it permits us to apply spectroscopic stability to the excited electronic manifold, that is, our zeroth moments are invariant to all unitary transformations over the excited state vibronic basis because the integrations in eq 4 are over the entire vibronic envelope of the electronic transition. Thus M_0/A_0 is invariant to all first-order effects in the excited state including spin−orbit, Jahn−Teller, and crystal field perturbations. In addition, M_0/A_0 is invariant to the displacement of the excited state surface along the ground state Jahn−Teller coordinate because we use complete sets of harmonic oscillators in our excited vibrational basis (Figure 8). Thus we may use the simple relation $|\langle\chi_0^l|\chi_{ex}\rangle_n|^2 = |\langle\chi_0^r|\chi_{ex}\rangle_n|^2$, i.e. we may use the solid rather than the dashed excited state surface in Figure 10 *to calculate the zeroth moment ratio*. We substitute the eqs 27 and 28 expressions weighted by appropriate Boltzmann factors into eqs 21, insert the latter into eq 1, and integrate over all frequencies remembering that $\int f_{n_1n_2n_3}(\mathcal{E})\,d\mathcal{E} = 1$. Noting that $\sum_n|\langle\chi_0^{l,r}|\chi_{ex}\rangle_n|^2 = 1$, the result is,

$$\frac{M_0}{A_0} = \frac{0.467}{kT}\sum_n \langle\chi_0^l|\chi_{ex}\rangle_n\langle\chi_0^r|\chi_{ex}\rangle_n\left[\bar{L}_z\gamma_{00} + \tanh\left(\frac{\zeta\bar{L}_z\gamma_{00}}{2kT}\right)\right] + K \tag{29}$$

and in accord with eq 4, $K \equiv 0.467\bar{\mathcal{B}}_0/\bar{\mathcal{D}}_0$. Furthermore, in summing over the Jahn−Teller vibrational quantum number, we note that

$$\sum_{n_{JT}=0}^{\infty}\langle\chi_0^l|\chi_{ex}\rangle_{n_{JT}}\langle\chi_0^r|\chi_{ex}\rangle_{n_{JT}} = \sum_{n_{JT}=0}^{\infty}(-1)^{n_{JT}}(\langle\chi_0^{l,r}|\chi_{ex}\rangle_{n_{JT}})^2 = e^{-\lambda^2_{JT}} = \gamma_{00} \tag{30}$$

The second equality in eq 30 is a well-known property of the Laguerre polynomials. Thus our final expression is

$$\frac{M_0}{A_0} = \frac{0.467}{kT}\gamma_{00}\left[\bar{L}_z\gamma_{00} + \tanh\left(\frac{\zeta\bar{L}_z\gamma_{00}}{2kT}\right)\right] + K \tag{31}$$

K represents the out-of-state $\bar{\mathcal{B}}$ term contribution.

To compare eq 31 with experiment, we carry out a nonlinear least-squares fit. The known quantities are $\bar{L}_Z = 1.33$ (from the Hückel calculation), $\zeta = 32$ cm^{-1}; the unknown parameters are λ_{JT} and K. The results are $\lambda_{JT} = 1.83$ and $K = 0.0048$. The corresponding fit is shown by the dashed curve in Figure 5 and is seen to be rather poor. But we have not yet considered another perturbation which must be present (aside from or in part due to the Cs^+ counterion which we discuss later), namely a crystal field, since COT^- clearly does not reside at a site of D_{8h} symmetry in an Ar matrix.

(b) Crystal Field Effects. We have consistently found crystal field (or site) splittings in previous work,[30,31] and they typically range from a few to ~100 cm^{-1}. Only crystal fields transforming as b_{1g} or b_{2g} in D_{8h} can split the ground state orbital degeneracy to first order. We consider the simplest case and add a crystal field of the same symmetry as the Jahn−Teller coordinate ($b_{1g}(D_{8h})$) to our Hamiltonian. The matrix of ($\hat{H}_{SO} + \hat{H}_{JT} + \hat{H}_{CF}$) in the basis of eq 24 is given in Table 4. The crystal field term (Δ) significantly complicates the calculation; the MCD becomes more complex because one now finds that (in-state) $\bar{\mathcal{B}}$ terms arise between the two Kramers doublets. In addition, though the ground state wave functions are still of the form of eq 26, c_1 and c_2, rather than having the value $2^{-1/2}$, are complicated functions of Δ, λ_{JT}, $\bar{L}_Z$, and ζ. Nonetheless, c_1 and c_2 are readily calculated by simply diagonalizing the first 2 × 2 matrix in Table 4. The splitting of the two Kramers doublets is now given by $[(\zeta\bar{L}_Z\gamma_{00})^2 + \Delta^2]^{1/2}$, and we recalculate the MCD and absorption in analogy to eqs 27 and 28. Recalculating the zeroth moment ratio, we obtain

$$\frac{M_0}{A_0} = 0.934\gamma_{00}\left[\frac{c_1c_2}{kT}\left(\tanh\left(\frac{W}{2kT}\right) + 2c_1c_2\bar{L}_Z\gamma_{00}\right) + \tanh\left(\frac{W}{2kT}\right)\frac{\bar{L}_Z\gamma_{00}}{W}(c_2^2 - c_1^2)^2\right] + K \tag{32}$$

where $W \equiv [(\zeta\bar{L}_Z\gamma_{00})^2 + \Delta^2]^{1/2}$.

Though this expression is complicated, it is perfectly straightforward to do a nonlinear least-squares fit, the result of which is shown as the solid curve in Figure 5. The fit is thereby substantially improved and now looks quite respectable. The one new parameter, Δ, has the value 13.5 cm^{-1}, and the value of λ_{JT} has decreased significantly from about 1.83 in the earlier fit to 1.59. Using these parameters, the splitting (W) between the ground state Kramers doublets is now calculated to be 13.9 cm^{-1}, much larger than in the absence of the crystal field (1.5 cm^{-1}), but still comparable to the kT range of our experiments ($\approx$1−15 cm^{-1}) and still small compared to experimental line widths.

We cannot claim to have demonstrated conclusively that a crystal field is present since the addition of a parameter will always improve the fit. We can say that a crystal field in the range observed in other matrix isolated conjugated systems[30,31] certainly improves the fit substantially. Perhaps more important, we can be quite confident that λ_{JT} is in the range 1.5−1.8 independent of crystal field considerations. With $\lambda_{JT} = 1.59$ and $\nu_{JT} = 1141$ cm^{-1}, our calculated ground state Jahn−Teller energy is $E_{JT} = {}^1/_2\,\lambda^2_{JT}h\nu_{JT} = 1442$ cm^{-1}, which is about 2.5 times the zero-point energy of the Jahn−Teller mode. This means that each COT^- anion in its ground electronic state is rather strongly trapped in one of two Kekule-like structures; tunneling between them is possible due to spin−orbit and crystal field perturbations. Though we have not explicitly observed the ground state Jahn−Teller frequency, it is interesting to note that Dvorak and Michl[17] report an 1120 cm^{-1} mode in their *fluorescence* (but not absorption) spectrum of COT^- in 2-methyltetrahydrofuran glass, in addition to the modes we have seen in this work. This observed 1120 cm^{-1} mode is of course a ground state frequency, and it agrees closely with the calculated ground state frequency of 1141 cm^{-1} (Table 2). This lends strong support to our choice of this mode and frequency as the Jahn−Teller active one.

(30) VanCott, T. C.; Rose, J. L.; Misener, G. C.; Williamson, B. E.; Schrimpf, A. E.; Boyle, M. E.; Schatz, P. N. *J. Phys. Chem.* **1989**, *93*, 2999.

(31) VanCott, T. C.; Koralewski, M.; Metcalf, D. H.; Schatz, P. N.; Williamson, B. E. *J. Phys. Chem.* **1993**, *97*, 7417.

6. The Role of The Cs^+ Ion. In our considerations thus far, we have completely ignored the presence of the Cs^+ ion. It seems clear both on electrostatic grounds and from any reasonable mechanism for the formation of COT^- that the Cs^+ and COT^- must be in close proximity in the matrix, probably as an ion pair in direct contact. We can state quite definitively that the Cs^+ ion must lie on or close to the C_8 axis of the COT^- anion, or more precisely, that any perturbation of the 8-fold symmetry of COT^- by the Cs^+ ion must be $\leq\sim 13$ cm^{-1} in view of our fit of the zeroth moment data. (Dvorak and Michl[17] also concluded that the counterions are located on 4-fold or 8-fold symmetry axes in their rigid solutions.) As we increase the crystal field parameter (Δ) in eq 32 holding other parameters fixed, the temperature dependence and magnitude of M_0 (or M_0/A_0) decreases monotonically and is down by almost an order of magnitude for $\Delta \sim 80$ cm^{-1}. Such a case seems applicable when Na atoms are used in place of Cs atoms to form COT^-. The spectra are less well resolved, and one finds[32] that the ratio of peak MCD to peak absorption is almost an order of magnitude smaller than for COT^-/Cs^+, and no MCD temperature dependence is observed over the range $\sim 1.7-10$ K. Why using Na in place of Cs makes so great a difference does not seem clear. In any event, it is entirely possible that the static crystal field we do observe using Cs ($\Delta \approx 13.5$ cm^{-1}) is due at least in part to an asymmetric placement of the Cs^+ ion with respect to the COT^- C_8 axis.

Let us now assume that the Cs^+ ion is exactly on the 8-fold axis of the average configuration of the COT^- ion. (Any deviation from this placement is simply regarded as a contribution to Δ.) We can for example picture the Cs^+ as a sphere lying in the trough of an eight-sided doughnut. In any such configuration, the symmetry is reduced to point group C_{8v}, and the question is whether any new features are thereby introduced into the previous analysis. To answer this, we consider the correlations between point groups D_{8h} and C_{8v}. The character table for C_{8v} may be obtained from that of D_{8h} by deleting the classes C'_2, C''_2, i, S_8, S_8^3, S_4, and σ_h, deleting all of the ungerade irreps and the g labels on the remaining irreps. One then finds that the C_{8v} character table is identical to the D_8 character table and thus these two groups are isomorphic. In effect, the C_{8v} character table is obtained from D_8 by replacing the classes C'_2 and C''_2 respectively by the classes σ_d and σ_v. The correlation of the gerade irreps of D_{8h} with those of C_{8v} is obtained by simply dropping the g subscripts while the correlation of the ungerade irreps is $A_{1u} \rightarrow A_2$, $A_{2u} \rightarrow A_1$, $B_{1u} \rightarrow B_2$, $B_{2u} \rightarrow B_1$, $E_{1u} \rightarrow E_1$, $E_{2u} \rightarrow E_2$, $E_{3u} \rightarrow E_3$. In C_{8v}, $[E_2^2] = a_1 \oplus b_1 \oplus b_2$, $[E_1^2] = a_1 \oplus e_2$, so the JT-active modes in the $^2E_2$ ground state are b_1 and b_2 (as compared to b_{1g} and b_{2g} in D_{8h}) and in the excited $^2E_1$ state they are e_2 (as compared to e_{2g} in D_{8h}). Thus as expected, all of the D_{8h} Jahn-Teller-active modes apply in C_{8v}. In addition, there are two D_{8h} out-of-plane b_{1u} modes which become formally Jahn–Teller-active in the $^2E_2(C_{8v})$ ground state and two D_{8h} out-of-plane e_{2u} modes which become formally active in the $^2E_1(C_{8v})$ (or $^2E_1(C_{4v})$) excited state. The calculated D_{8h} frequencies of these modes are given in Table 2. While we cannot rigorously exclude the possibility that one of the D_{8h} b_{1u} modes is the Jahn–Teller-active mode rather than the Kekule-like b_{1g} (D_{8h}) mode employed in our treatment above, both chemical intuition and the fact that the former only becomes active to the extent that the Cs^+ perturbs the COT^- ring, strongly favors our original choice, as does the Dvorak and Michl[17] observation of the 1120 cm^{-1} mode mentioned above. Finally, the presence of the Cs^+ ion adds three additional modes to the system; these belong to irreps $a_1 \oplus e_1$. The former adds a third totally symmetric mode to the system, namely the Cs^+ vibrating against the COT^- ring, but this frequency is expected at a frequency ≤ 200 cm^{-1}.

We conclude that the presence of the Cs^+ ion does not significantly alter our previous analysis.

V. Conclusions

The MCD and absorption spectra of cyclooctatetraene mononegative ion prepared by co-condensing Cs and cyclooctatetraene in an Ar matrix can be understood if it is assumed that the ground state is $^2E_{2u}(D_{8h})$ perturbed by Jahn–Teller, spin–orbit, and crystal field effects. In addition, it is necessary to assume that the excited state electronic symmetry is lower than D_{8h}, the two possibilities being D_{4h} or D_{2d}. There is significant Jahn–Teller coupling in the excited electronic state as well as coupling to two totally symmetric modes. The ground state molecular parameters are determined by the magnitude and temperature dependence of the MCD as expressed by the ratio of MCD and absorption zeroth moments whereas the overall absorption and MCD band patterns are determined by the excited state vibronic coupling parameters.

The ground state parameters are $\nu_{JT}(b_{1g}) \approx 1140$ cm^{-1}, $\lambda_{JT} \approx 1.6$, $E_{JT} \approx 1440$ cm^{-1}, and crystal field $\Delta(b_{1g}) \approx 13$ cm^{-1}. The ground state orbital angular momentum is strongly Ham-effect quenched by the factor $e^{-\lambda^2_{JT}} \approx 0.08$. In the ground state, the molecule can be pictured as strongly trapped in either of two equivalent Kekule-like configurations, with zero-point energy about 40% of the potential barrier separating the two configurations. Because of the presence of crystal field and spin–orbit perturbations, tunneling between the two structures is permitted.

In the excited D_{4h} (or D_{2d}) state, the equilibrium configuration is Kekule-like and the Jahn–Teller mode is an in-plane motion in which the molecule is squashed, for example, along the x-axis and elongated along the y-axis, and vice versa as illustrated in the middle panel of Figure 6. The excited state Jahn–Teller parameters are $\nu_{JT} = 270$ cm^{-1}, $\lambda_{JT} = 0.99$, $E_{JT} = 132$ cm^{-1}; the molecule can move freely between Jahn–Teller minima.

Acknowledgment. This work was supported by the National Science Foundation under Grants CHE8902456, CHE9207886 (P.N.S.), and CHE8516611 (L.A.). P.N.S. thanks the Department of Chemistry, University of Canterbury, New Zealand, for their gracious hospitality and the University of Canterbury for the award of a Visiting Erskine Fellowship during which a portion of this manuscript was written. He also acknowledges many incisive discussions with Dr. Bryce E. Williamson during that period and thanks Dr. Robert Maclagan, University of Canterbury, for performing the Gaussian-90 calculation of the vibrational frequencies of cyclooctatetraene mononegative ion. Some of the Jahn–Teller calculations were made possible by a grant of time to S.B.P. by the Pittsburgh Supercomputer Center.

(32) Samet, C. Ph.D. Dissertation, Department of Chemistry, University of Virginia, August, 1988.

(33) Griffith, J. S. *The Theory of Transition-Metal Ions*; University Press: Cambridge, 1964.